Nucleon density in the nuclear periphery determined with antiprotonic x rays: Cadmium and tin isotopes

R. Schmidt,[1] A. Trzcińska,[2] T. Czosnyka,[2] T. von Egidy,[1] K. Gulda,[3] F. J. Hartmann,[1] J. Jastrzębski,[2] B. Ketzer,[1] M. Kisieliński,[2] B. Kłos,[4] W. Kurcewicz,[3] P. Lubiński,[2,*] P. Napiorkowski,[2] L. Pieńkowski,[2] R. Smolańczuk,[5] E. Widmann,[6] and S. Wycech[5]

[1]*Physik-Department, Technische Universität München, D-85747 Garching, Germany*
[2]*Heavy Ion Laboratory, Warsaw University, PL-02-093 Warsaw, Poland*
[3]*Institute of Experimental Physics, Warsaw University, PL-00-681 Warsaw, Poland*
[4]*Physics Department, Silesian University, PL-40-007 Katowice, Poland*
[5]*Sołtan Institute for Nuclear Studies, PL-00-681 Warsaw, Poland*
[6]*CERN, CH-1211, Geneva 23, Switzerland*
(Received 20 June 2002; published 28 April 2003)

The x-ray cascade from antiprotonic atoms was studied for ^{106}Cd, ^{116}Cd, ^{112}Sn, ^{116}Sn, ^{120}Sn, and ^{124}Sn. Widths and shifts of the levels due to strong interaction were deduced. Isotope effects in Cd and Sn isotopes were investigated. The results are used to determine the nucleon density in the nuclear periphery. The deduced neutron distributions are compared with the results of the previously introduced radiochemical method and with Hartree-Fock-Bogoliubov calculations.

I. INTRODUCTION

Antiprotonic atoms are a specific tool to study the strong interaction and the nucleon density at the nuclear periphery. The strong-interaction potential leads to widths and energy shifts of antiprotonic-atom levels in addition to the pure electromagnetic interaction. The measurement of these widths and shifts gives information on the strength of the interaction, which is often expressed by an effective scattering length in the optical potential model [1], and on the nucleon density in the region where annihilation takes place.

In contrast to other methods which are sensitive to the charge distribution and usually probe the whole nucleus with the nuclear periphery giving only a small contribution, antiprotons are sensitive to the matter density at the nuclear periphery (they probe the nucleon density at distances about 2 fm larger than the half density charge radius). By investigating different isotopes of one element, the effect of additional nucleons can be deduced. The major part of the effect comes from the higher nucleon density in the nuclear periphery of isotopes with more neutrons [2]. Isospin effects on the effective antiproton-nucleon scattering length may also exist.

Prior to the present study, data on antiprotonic atoms were collected for several elements [3]. However, with a few exceptions, these were mainly light isotopes ($Z<40$) and a number of them was investigated using natural targets under difficult antiproton beam conditions. The aim of the PS209 Collaboration was to measure with antiprotons from LEAR at CERN a large variety of elements and isotopes in order to provide a set of data for a new combined analysis to determine the nucleon density in the nuclear periphery [4]. This

analysis is expected to yield data about the neutron density in the annihilation region and a better knowledge of the antiproton-nucleus interaction, e.g., about the density or isospin dependence of the effective scattering length [3,5].

The results of the PS209 experiment were reported at a number of conferences, see, e.g., Refs. [6–8]. In particular, the last reference presents a comprehensive table of level widths and shifts determined in 34 monoisotopic or isotopically separated targets ranging from ^{16}O to ^{238}U. In Ref. [9] these data were analyzed under the assumption of a two-parameter Fermi (2pF) distribution of peripheral protons and neutrons. A linear relationship of the difference between the neutron and proton root mean square radii (rms) Δr_{np} and the asymmetry parameter $\delta=(N-Z)/A$ was established (where N, Z, and A are neutron, atomic, and mass numbers, respectively). Besides conference communications, more detailed reports on the evaluations of PS209 results have been published [10,11] or are currently in preparation. Here results for tin and cadmium isotopes are presented. The isotopes ^{106}Cd, ^{116}Cd, ^{112}Sn, ^{116}Sn, ^{120}Sn, and ^{124}Sn have been investigated. For four of these nuclei also the neutron-to-proton density ratio in the nuclear periphery could be measured using the radiochemical method [12–15].

II. EXPERIMENTAL METHOD AND SETUP

The principle of the method employed is described in Ref. [10]. The antiprotons are captured into a high antiprotonic-atom orbit. They cascade down towards levels with lower principal quantum number $n_{\bar{p}}$ by the emission of Auger electrons and x rays. In states with low $n_{\bar{p}}$, the orbit of the antiproton comes close to the nucleus and the interaction with the nucleus becomes large. The resulting shifts and widths of the levels were partly evaluated and interpreted as explained in the following sections.

The strong-interaction width can be measured directly

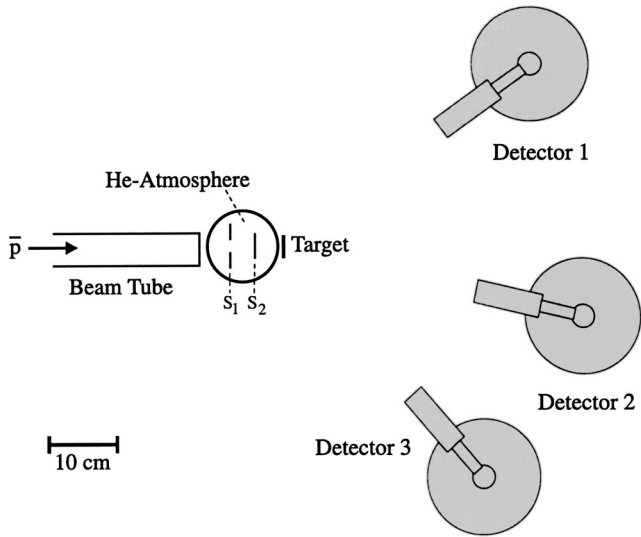*Present address: N. Copernicus Astronomical Center, 00-716 Warsaw, Poland.

FIG. 1. Schematic view of the experimental setup: S_1, anti-counter and S_2, counter of the telescope.

TABLE I. Target properties: thickness d, enrichment a, number of antiprotons used, and on-line calibration sources.

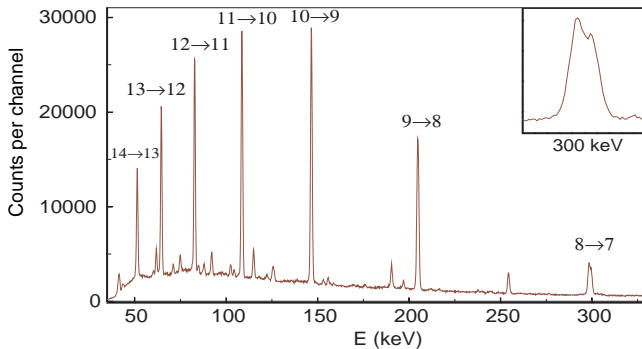| Target	d (mg/cm^2)	a (%)	number of $\bar{p}$ (10^8)	Calibration sources
^{106}Cd	40.0	76.5	9	^{137}Cs, ^{152}Eu
^{116}Cd	64.5	93.0	10	^{137}Cs, ^{152}Eu
^{112}Sn	65.6	94.7	17	^{137}Cs, ^{152}Eu
^{116}Sn	46.8	93.0	9	^{137}Cs, ^{152}Eu
^{120}Sn	65.3	99.2	11	^{137}Cs, ^{152}Eu
^{124}Sn	70.1	97.9	23	^{133}Ba, ^{137}Cs, ^{152}Eu

FIG. 2. Antiprotonic x-ray spectrum from ^{124}Sn measured with detector 1. The inset shows the spectrum around the transition $n=8\rightarrow7$.

TABLE II. Measured antiprotonic x-ray intensities, normalized to 100 transition $n=11\rightarrow10$ (mean values of the results from three detectors).

Transitions		Energy (keV)	^{106}Cd	^{116}Cd
8→7		276	72.70±2.79	75.64±2.84
9→8		188	119.01±6.24	114.53±5.80
10→9	13→11	135	131.46±6.62	132.17±6.98
11→10		100	100.00±5.04	100.00±5.81
12→11		76	83.28±4.21	84.46±6.95
13→12		59	66.35±3.42	66.66±8.10
14→13	18→16	47	54.54±2.99	56.03±10.9
9→7		464	5.38±0.95	5.00±0.64
10→8		323	11.71±0.74	11.53±0.76
11→9	13→10	234	22.78±1.20	20.97±1.12
12→10		175	18.40±3.61	17.30±0.92
14→12		106	13.64±0.74	13.96±0.86
15→13		84	10.27±0.58	10.54±0.77
16→14		68	6.10±0.38	7.18±0.74
17→15		56	12.09±0.68	10.99±1.52
19→17		39	9.97±1.0	18.38±7.20
11→8	7→6	423	5.59±0.69	3.72±0.53
12→9		310	3.81±0.39	4.41±0.43
14→11		181	5.09±0.92	5.72±0.37
15→12		143	4.22±0.31	4.2±0.5
16→13	18→14	115	5.16±0.36	5.20±0.37
17→14		94	6.29±0.40	6.23±0.48
18→15		78	3.84±0.33	4.83±0.45
19→16		65	2.5±0.5	2.82±0.37
12→8		498	1.28±0.46	1.30±0.53
13→9		369	1.30±0.38	2.17±0.33
14→10		281	1.86±0.55	1.83±0.25
15→11		219	2.33±0.31	1.83±0.25
16→12		174	0.99±0.79	1.81±0.36
17→13		141	2.6±0.26	2.81±0.26
19→15		96	2.73±0.26	2.7±0.5
17→12		200	2.0±0.5	2.01±0.27
18→13		162	1.79±0.24	1.69±0.23
19→14		133	1.97±0.32	1.81±0.75

(via analysis of the line shape) if it is of the order of magnitude of the instrumental resolution (about 1 keV). For many isotopes this is the case for the lowest visible transition. The energy of the transitions may be measured with an accuracy of about 10 eV. Thus strong-interaction energy shifts which are larger than this value may be determined. For those levels, for which the strong-interaction width is of the order of the electromagnetic width (due to x ray and Auger transitions), the strong-interaction width was deduced from the intensity balance of the x-ray transitions feeding and depopulating the respective level [16]. In the case of noncircular

TABLE III. Measured antiprotonic x-ray intensities, normalized to 100 transition $n=11\rightarrow10$ (mean values of the results from three detectors).

Transitions		Energy (keV)	^{112}Sn	^{116}Sn	^{120}Sn	^{124}Sn
8→7		299	70.71±2.67	65.35±4.90	60.82±2.20	56.19±2.51
9→8		205	114.64±5.77	114.72±5.78	113.10±5.76	110.00±5.53
10→9	13→11	146	128.09±6.58	125.66±6.38	126.99±6.51	126.26±6.48
11→10		108	100.00±5.44	100.00±5.10	100.00±5.43	100.00±5.61
12→11		82	82.68±5.26	83.21±4.50	84.06±5.33	83.95±5.75
13→12		64	68.96±6.27	70.42±4.45	72.49±6.61	72.97±7.26
13→14	18→16	51	57.39±7.57	59.83±4.93	61.39±8.05	61.55±8.85
15→14		41	26.38±5.34	27.33±3.26	31.55±6.33	29.47±6.52
9→7		503	4.15±0.31	4.56±1.0	3.69±0.34	3.52±0.26
10→8		350	12.03±0.67	11.55±0.64	11.81±0.69	11.56±0.77
11→9	13→10	255	18.92±1.17	19.54±1.99	18.83±2.05	16.86±1.50
12→10	16→12	190	14.41±0.75	13.96±0.73	14.15±0.74	13.42±0.70
14→12		115	12.00±0.67	12.02±0.64	12.26±0.68	12.40±6.92
15→13		92	8.54±0.54	8.72±0.48	8.74±0.54	8.49±0.54
16→14		74	6.57±0.53	6.56±0.41	5.29±0.52	6.20±0.59
17→15		61	10.49±1.04	11.23±0.78	11.56±1.12	11.79±1.29
19→17		43	6.59±1.25	5.73±0.71	8.38±1.65	6.26±1.32
11→8		458	2.03±0.20	1.7±0.5	1.76±0.19	1.58±1.0
12→9		336	4.13±0.29	4.11±0.31	3.86±0.27	3.16±0.22
14→11		197	4.53±0.29	3.89±0.32	4.43±0.28	4.68±0.26
15→12		156	3.5±0.5	3.0±0.5	3.75±0.22	3.62±0.21
16→13	18→14	125	3.71±0.27	3.92±0.25	4.15±0.25	3.9±1.0
17→14		102	5.05±0.31	4.60±0.27	4.47±0.27	4.83±0.30
18→15		84	3.20±0.24	3.18±0.22	3.29±0.24	2.76±0.22
19→16		71	2.49±0.23	2.86±0.19	3.14±0.28	3.61±0.33
13→9		400	1.56±0.18	1.72±0.19	1.61±0.16	1.15±0.13
14→10		305	1.12±0.14	0.98±0.16	1.41±0.15	1.18±0.17
15→11		238	1.92±0.15	1.83±0.17	1.49±0.14	1.69±0.14
17→13		153	2.43±0.17	2.13±0.16	1.96±0.14	2.24±0.15
19→15		104	1.45±0.14	1.33±0.13	1.28±0.12	1.3±1.0

transitions the feeding transitions cannot be observed experimentally, as they are hidden by the much stronger intensities of the circular transitions. In these cases, the feeding intensities can be taken from cascade calculations if the cascade is sufficiently well known [10].

The experiment was performed with the antiproton beam provided by LEAR of CERN. The setup (cf. Fig. 1) is similar to that described in Ref. [10]. Due to the small initial momentum of the antiprotons of 106 MeV/c (6 MeV energy) the scintillation-counter telescope (consisting of an anticounter $S1$ and a counter $S2$) was placed inside a chamber (with aluminum windows of thickness 12 μm) filled with helium to avoid large energy losses in air. After passing the chamber window the antiprotons were stopped inside the target. The properties of the different targets are listed in Table I.

The x rays emitted during the antiproton cascade were measured with three Ge detectors (two coaxial detectors with an active diameter of 49 mm and a length of 50 mm, and one planar detector with diameter 36 mm and thickness 14 mm) with a resolution of about 1 keV at 200 keV γ-ray energy. The detectors were placed at distances of about 50 cm from the target at angles of 13°, 35°, and 49° towards the beam axis, respectively. The detector-target distance was adjusted so as to obtain a good signal-to-noise ratio and simultaneously decrease the background produced by pions from the annihilation processes. It was necessary as the pions depose a larger energy than x rays do, and so enlarge detector dead time significantly. This also allowed us to avoid summing effects (simultaneous detection of two x-ray transitions). The x rays were measured in coincidence with the antiproton signal in a time window which was extended up to 500 ns after the antiproton signal from the telescope counter. The stability and efficiency of the detectors and the data acquisition system were checked by on-line and off-line measurements with calibration sources.

TABLE IV. Radiative width Γ_{em} and Auger width Γ_{Auger} for those levels of $\bar{p}$-Cd where the strong-interaction width was determined via the intensity balance. Values in eV.

	^{106}Cd		^{116}Cd	
(n,l)	Γ_{em}	Γ_{Auger}	Γ_{em}	Γ_{Auger}
(8,7)	4.95	0.04	4.70	0.04
(9,7)	3.49	0.06	3.31	0.05
(7,6)	9.86	0.03		

III. EXPERIMENTAL RESULTS

The x-ray spectrum from the target ^{124}Sn, as taken with detector 1, is shown in Fig. 2. Those lines in the spectra which are not significantly broadened by strong interaction were fitted with Gaussians. Their relative intensities are given in Tables II and III for the Cd and Sn isotopes, respectively. For the fit of the transition $n=8\rightarrow7$, two Lorentzians convoluted with Gaussians were used. The strong-interaction energy shifts are defined as the difference between the energy calculated with a purely electromagnetic potential [17] and the measured transition energy.

The widths of the levels $(n,l)=(8,7)$ were determined from the measured intensity balance. Small corrections for parallel transitions and for unobserved transitions from higher levels were taken from the calculated cascade [10]. For the determination of the width of the level (9,7) all intensities of the feeding transitions were taken from the results of the cascade calculations. The radiative and Auger widths (obtained according to Ref. [18]) which were used for these calculations are summarized in Table IV for cadmium and in Table V for tin. Tables VI and VII give the measured widths and shifts for the cadmium and tin isotopes, respectively. The variation of these observables due to the different number of protons and neutrons from ^{106}Cd to ^{124}Sn is clearly visible. The widths for ^{124}Sn are roughly twice as large as those for ^{106}Cd. The shifts turn from attractive or compatible with zero for ^{106}Cd to repulsive for ^{124}Sn. The only observable which does not follow the rather smooth variation is the upper level $(n,l=8,7)$ width of ^{106}Cd. For all other nuclei presented in these tables the ratio of lower to upper level widths is $\Gamma_{low}/\Gamma_{up}=85\pm7$, whereas the same ratio is only about 50 in case of ^{106}Cd.

This effect is due to the $E2$ resonance [19], which in Cd nuclei mixes the $n,l=6,5$ and the $n,l=8,7$ states. The difference between the energies of the nuclear 2^+ state and the corresponding antiprotonic-atom transition is 65 keV and 184 keV in ^{106}Cd and ^{116}Cd, respectively. As the electric

quadrupole moment is not very different for both nuclei [20], the increase of the upper level width due to the mixing is more significant in ^{106}Cd than in ^{116}Cd. This qualitatively explains the observed effect.

To be more quantitative, the width of the $n,l=6,5$ level in Cd nuclei should be known. This width was estimated by an extrapolation to $Z=48$ of the systematics presented in Ref. [21] for lower Z nuclei [a semiempirical curve $\Gamma(Z)$ of the form $\log(\Gamma)=a+bZ+cZ^2$, where Z is the atomic number, was fitted to the set of widths of level $n=6$]. The extrapolated value is 7.7 ± 2.5 keV. With the optical potential of Ref. [3] we calculated the $(n,l=6,5)$ level widths (shifts) to be 8.2 keV (2.2 keV) for ^{106}Cd and 9.5 keV (2.7 keV) for ^{116}Cd. To correct the experimental $n=8$ level width the calculated rather than the extrapolated values were used with an adopted error of 15%. This leads to an $E2$ induced width of 2.4 ± 0.3 eV and 0.40 ± 0.04 eV in ^{106}Cd and ^{116}Cd, respectively. A summary of the measured values for ^{106}Cd is shown in Fig. 3.

The $E2$ resonance effect, mixing the $(n,l=7,6)$ and $(n,l=5,4)$ wave functions, was also found for the Cd and Sn nuclei. The widths and shifts of the $(n,l=5,4)$ level needed for the correction were calculated in the same way as for the $(n,l=6,5)$ level in Cd. The corrected values of the level widths and shifts (presented in Tables VI and VII) were used for the calculations given in Table VIII and discussed in the following section.

IV. DISCUSSION

The region of tin isotopes with the closed $Z=50$ proton shell constitutes one of the favorable parts of the nuclear chart for experimental and theoretical nuclear-structure studies. During our investigation on antiprotonic atoms in this region we also measured, besides the results reported in this paper, the level widths and shifts in even Te isotopes ($Z=52$) [22]. In addition, using the radiochemical method [12], we have determined the neutron halo factor, a quantity reflecting the composition of the outer nuclear periphery in ^{106,116}Cd, ^{112,124}Sn [14,15], and in ^{128,130}Te [14].

In the present discussion, we will concentrate on the first two elements. In our recent publication [9], we presented in detail our method to determine the peripheral neutron distribution and differences between the neutron and proton mean square radii Δr_{np} using observables gathered from antiprotonic atoms under the assumption of a 2pF neutron and proton distributions, $\rho(r)=\rho_0\{1+\exp[(r-c)/a]\}^{-1}$. Here c is the half density radius, a the diffuseness parameter (related to the surface thickness t by $t=4\ln 3\, a$) and ρ_0 is a normal-

TABLE V. Radiative width Γ_{em} and Auger width Γ_{Auger} for those levels of $\bar{p}$-Sn where the strong-interaction width was determined via the intensity balance. Values in eV.

	^{112}Sn		^{116}Sn		^{120}Sn		^{124}Sn	
(n,l)	Γ_{em}	Γ_{Auger}	Γ_{em}	Γ_{Auger}	Γ_{em}	Γ_{Auger}	Γ_{em}	Γ_{Auger}
(8,7)	5.79	0.04	5.67	0.04	5.56	0.04	5.46	0.04
(9,7)	4.08	0.06	3.99	0.06	3.92	0.06	3.85	0.05

TABLE VI. Measured level widths and shifts for the cadmium isotopes (LS components and average values). Values in eV.

| | ^{106}Cd | | ^{116}Cd | |
	$j=l+1/2$	$j=l-1/2$	$j=l+1/2$	$j=l-1/2$
$\Gamma(7,6)$	173 ± 83	229 ± 86	307 ± 63	186 ± 69
		199 ± 60		251 ± 47
$\Gamma(7,6)$ [a]		196 ± 60		248 ± 47
$\epsilon(7,6)$	-32 ± 27	-20 ± 29	-15 ± 22	-24 ± 24
		-26 ± 20		-19 ± 16
$\epsilon(7,6)$ [a]		-36 ± 20		-29 ± 16
$\Gamma(8,7)$	3.5 ± 0.7	4.2 ± 0.8	2.7 ± 0.6	3.3 ± 0.7
		3.8 ± 0.5		3.0 ± 0.5
$\Gamma(8,7)$ [a]		1.4 ± 0.6		2.6 ± 0.5
$\Gamma(9,7)$		17^{+20}_{-10}		18^{+19}_{-7}

[a]After the correction for the $E2$ effect (see text).

ization factor. This approach is summarized below.

Assuming identical annihilation probabilities on neutrons and protons, the radiochemical experiment determines the halo factor, which is close to the normalized neutron-to-proton density ratio $(Z\rho_n/N\rho_p)$ at a radial distance 2.5 ± 0.5 fm larger than the half density charge radius. Comparing the halo factor with the neutron-to-proton density ratio deduced from Δr_{np} as determined in other experiments, one can conclude that for neutron-rich nuclei it is mostly the neutron diffuseness that increases and not the half density radius [9]. Although this conclusion was based on the very simple 2pF model of the nuclear periphery, it is corroborated by the much more sophisticated Hartree-Fock-Bogoliubov (HFB) calculations. This is illustrated in Figs. 4 and 5, where the proton and neutron density distributions for ^{124}Sn are compared with both models. The HFB calculations were performed using the SkP force [23] and give a Δr_{np} value equal to 0.16 fm. As the calculated proton c_p and neutron c_n half density radii are almost identical, this rms difference is mainly due to the difference in the proton and neutron surface diffuseness. The fitted 2pF distributions with the HFB c_n, c_p, and Δr_{np} values closely approximate the HFB distributions. In the peripheral region from 6.5 fm to 8.5 fm, e.g., the 2pF neutron distribution differs by less than 20%

from that derived from HFB calculations. A similar result was obtained for other nuclei.

The antiprotonic x rays are analyzed using an optical potential with the antiproton-nucleon scattering length of the form $\bar{a}=(2.5\pm0.3)+i(3.4\pm0.3)$ fm, as proposed for point-like nucleons in Ref. [3]. The method allows us to study the nuclear density at radial distances of about 1 fm closer to the nuclear center than those examined in the radiochemical experiment.

The peripheral bare proton densities in the form of 2pF distributions are obtained [9] from experiments sensitive to the nuclear charge: electron scattering [24] or muonic x rays [25]. The differences between experimental level widths and shifts and those calculated with parameters of the proton distributions are attributed to the neutron contributions to these observables. Based on the analysis and the comparison described above, the half density radii of the proton and neutron distributions are assumed to be equal, $c_n=c_p$. The neutron diffuseness is considered as a free parameter, adjusted to agree best with the experimental lower and upper level widths (the lower level shifts were not included in the fits, see comments below).

Table VIII illustrates this procedure for the Cd and Sn

TABLE VII. Measured level widths and shifts for the tin isotopes (LS components and average values). Values in eV.

| | ^{112}Sn | | ^{116}Sn | | ^{120}Sn | | ^{124}Sn | |
	$j=l+1/2$	$j=l-1/2$	$j=l+1/2$	$j=l-1/2$	$j=l+1/2$	$j=l-1/2$	$j=l+1/2$	$j=l-1/2$
$\Gamma(7,6)$	411 ± 22	358 ± 25	386 ± 27	377 ± 31	448 ± 27	505 ± 32	493 ± 25	534 ± 29
		387 ± 17		382 ± 20		474 ± 21		512 ± 19
$\Gamma(7,6)$ [a]		358 ± 19		365 ± 20		397 ± 30		419 ± 24
$\epsilon(7,6)$	-9 ± 16	-1 ± 13	12 ± 18	36 ± 19	26 ± 17	37 ± 20	26 ± 17	63 ± 16
		-5 ± 11		23 ± 13		31 ± 13		43 ± 11
$\epsilon(7,6)$ [a]		26 ± 11		46 ± 13		61 ± 14		54 ± 17
$\Gamma(8,7)$	$4.1^{+0.8}_{-0.7}$	$4.3^{+0.8}_{-0.7}$	$4.7^{+1.4}_{-1.1}$	$5.2^{+1.5}_{-1.2}$	$4.9^{+0.8}_{-0.7}$	$6.4^{+1.0}_{-0.8}$	$5.5^{+1.0}_{-0.9}$	$6.8^{+1.1}_{-1.0}$
		4.2 ± 0.6		4.9 ± 0.9		5.6 ± 0.6		6.1 ± 0.7
$\Gamma(9,7)$		20^{+13}_{-6}		17^{+12}_{-6}		22^{+12}_{-6}		24^{+15}_{-7}

[a]After the correction for the $E2$ effect (see text).
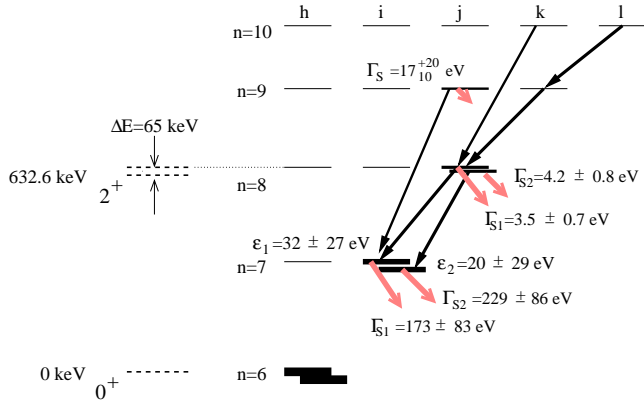
FIG. 3. Summary of measured shifts and widths for ^{106}Cd and the excitation energy of the nuclear 2^+ state in this nucleus. (All values are before correction for the $E2$ effect.)

FIG. 4. Comparison of the HFB model (dashed lines) and the two-parameter Fermi (2pF) density distributions (solid lines) for the nucleus ^{124}Sn. The 2pF distributions were fitted to HFB model curves (half density radii $c_n = c_p = 5.55$ fm and the difference between neutron and proton rms radii, $\Delta r_{np} = 0.16$ fm). The obtained 2pF diffuseness parameters are $a_p = 0.45$ fm and $a_n = 0.57$ fm.

nuclei. For the Sn nuclei the 2pF charge distribution determined using data from muonic atoms or from electron scattering differ significantly. Only the electron-scattering data lead to Δr_{np} values compatible with the systematics established for other nuclei [9] and with previous experiments [26,27]. Therefore, these data were retained for further analysis. In Fig. 6 the widths and shifts, calculated with the density distributions from this table and the scattering lengths given above, are compared with the corresponding experimental values. It is evident that the potential used is able to reproduce simultaneously the lower and upper level widths for Cd and Sn nuclei, whereas there are problems with the level shifts.

The analysis of the x-ray data as presented in Table VIII allows us to determine the normalized neutron-to-proton density ratio $Z\rho_n/N\rho_p$ as a function of the radial distance at the periphery of the investigated nuclei. As indicated above, the radiochemical experiment can be considered as giving the same ratio at a radial distance in the far periphery. Figure 7 compares the results of these two experiments, together with the normalized neutron-to-proton density ratio obtained from the HFB calculations. For the sake of illustration the comparison is extended to some other nuclei not discussed in
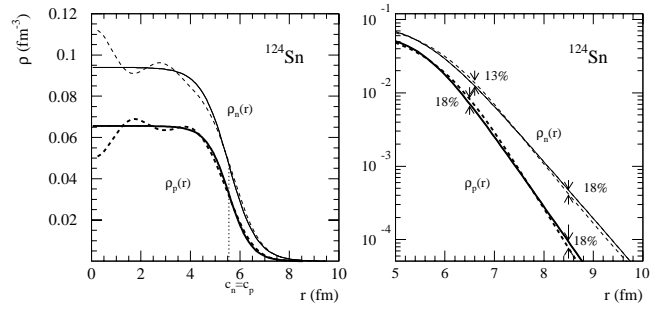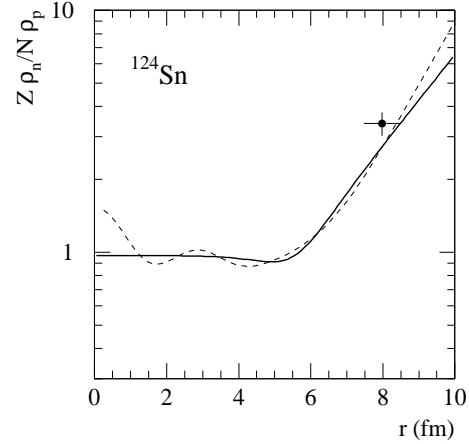

FIG. 5. The same as for Fig. 4 but for the density ratio $(Z\rho_n/N\rho_p)$. The cross indicates the halo factor measured in the radiochemical experiment [15].

TABLE VIII. Parameters of 2pF neutron density distributions deduced from the widths of antiprotonic levels in Cd and Sn atoms (in fm). c_{ch}, t_{ch}—the half density radius and the surface thickness of charge density distributions. c_p, t_p—the half density radius and the surface thickness of pointlike proton density distributions. Δt_{np}—difference of the surface thicknesses of proton and neutron distributions.

|	Charge distributions [a] from muonic atoms						Charge distributions [b] from electron scattering					
Isotope	c_{ch}	t_{ch}	c_p	t_p	Δt_{np}	χ^2	Δr_{np}	c_{ch}	t_{ch}	c_p	t_p	Δt_{np}	χ^2	Δr_{np}
^{106}Cd	5.2875	2.30	5.329	1.995	$0.30^{+0.25}_{-0.43}$	0.6	$0.10^{+0.10}_{-0.14}$							
^{116}Cd	5.4164	2.30	5.457	1.995	$0.45^{+0.10}_{-0.13}$	0.2	0.15 ± 0.04	5.42	2.34	5.461	2.043	$0.39^{+0.11}_{-0.13}$	0.2	$0.13^{+0.05}_{-0.04}$
^{112}Sn	5.3714	2.30	5.412	1.995	$0.48^{+0.04}_{-0.05}$	0.1	0.17 ± 0.01	5.375	2.416	5.416	2.184	$0.20^{+0.04}_{-0.06}$	0.3	0.07 ± 0.02
^{116}Sn	5.417	2.30	5.458	1.995	$0.44^{+0.06}_{-0.07}$	0.5	$0.15^{+0.02}_{-0.03}$	5.358	2.420	5.399	2.135	0.29 ± 0.07	0.6	0.10 ± 0.03
^{120}Sn	5.459	2.30	5.499	1.995	$0.48^{+0.08}_{-0.09}$	1.0	0.16 ± 0.03	5.315	2.530	5.356	2.263	$0.22^{+0.08}_{-0.10}$	1.0	$0.08\pm^{+0.03}_{-0.04}$
^{124}Sn	5.491	2.30	5.531	1.995	$0.47^{+0.07}_{-0.08}$	1.1	0.16 ± 0.03	5.490	2.347	5.530	2.052	$0.40^{+0.07}_{-0.09}$	1.1	0.14 ± 0.03

[a]Reference [25].
[b]Reference [24].
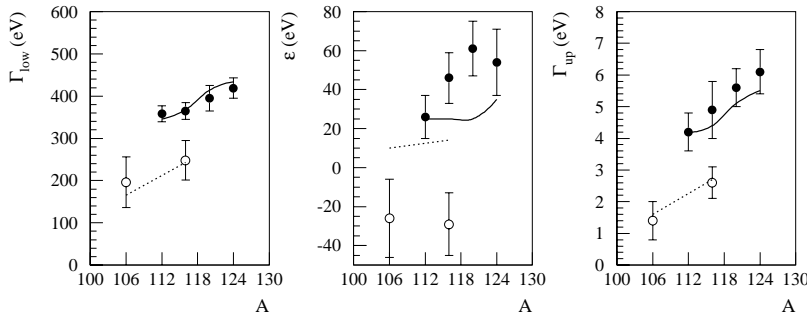
FIG. 6. Average widths and shifts of the levels (7,6), and widths of the levels (8,7) plotted versus A. Open circles and dotted lines, cadmium isotopes (all experimental data are corrected for the $E2$ effect). Full circles and solid lines, tin isotopes. The lines are calculated using the optical potential for pointlike nucleons [3] with the surface parameters given in Table VIII (see also text). Positive level shift corresponds to repulsive interaction.

detail in the present publication. For heavy Cd and Sn nuclei, the two experimental approaches are consistent within the experimental errors. They are also in fair agreement with HFB calculations. A similar result is obtained for 15 other investigated nuclei, partly shown in Fig. 7.

As already mentioned in our previous paper [9], the situation is quite different for the lightest members of the Cd and Sn chains. For these nuclei the analysis of the x-ray data gives densities consistent with the HFB model with Skyrme interaction as well as with recent calculations with Gogny forces [28]. The radiochemical experiment, however, seems to indicate a proton-rich nuclear periphery. We encountered a similar problem for the two lightest members of the Ru and Sm isotopic chains. In Ref. [5] the role of a quasibound $\bar{p}p(^{13}P_0)$ state in nuclei with weakly bound protons was indicated as an explanation of this puzzle. (For ^{106}Cd and

^{112}Sn the corresponding proton separation energies are 7354 keV and 7559 keV, respectively.) The formation of such a state would favor annihilation on protons in comparison with that on neutrons and would lead to a much smaller halo factor than really expected from the peripheral neutron and proton densities. This explanation, although opening new research areas, would indicate that our radiochemical method is not as universal as we believed previously.

The x-ray data, combined with proton distributions deduced from electron-scattering experiments (Sn nuclei) and muonic atoms (Cd nuclei) allowed us to determine the differences Δr_{np} between neutron and proton rms radii. The results are presented in Table VIII and in Fig. 8. The Δr_{np} value for ^{106}Cd is presented for the first time. The values for ^{116}Cd and ^{112,116,120,124}Sn are lower than those given in Ref. [9] as the correction for the $E2$ effect in these nuclei is now included. As may be seen in Fig. 8 the new, corrected Δr_{np} values are in reasonable agreement with previously presented systematics, although the isotopic effects in Sn nuclei are less pronounced than those reported in Ref. [9].

Before concluding this section we wish to emphasize that the Δr_{np} values given in the present work as well as in the previously published systematics [9] strongly depend on the charge distribution determined with electromagnetic probes.
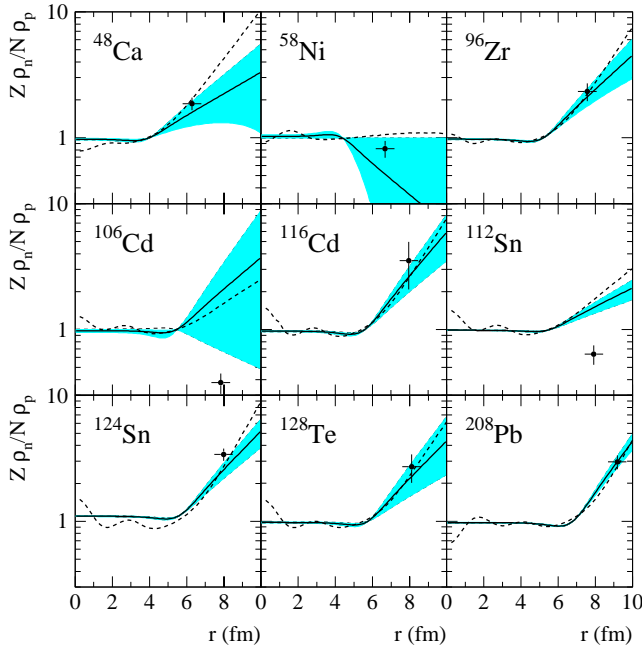

FIG. 7. Normalized neutron-to-proton density ratio ($Z\rho_n/N\rho_p$) deduced from strong-interaction level widths and shifts (solid lines with indicated statistical errors) and charge distributions given in Ref. [24] (Sn nuclei) and Ref. [25] (other nuclei). They are compared with f_{halo} measured in the radiochemical experiments (marked with crosses at a radial distance corresponding to the most probable annihilation site) and with HFB model calculations (dashed lines).
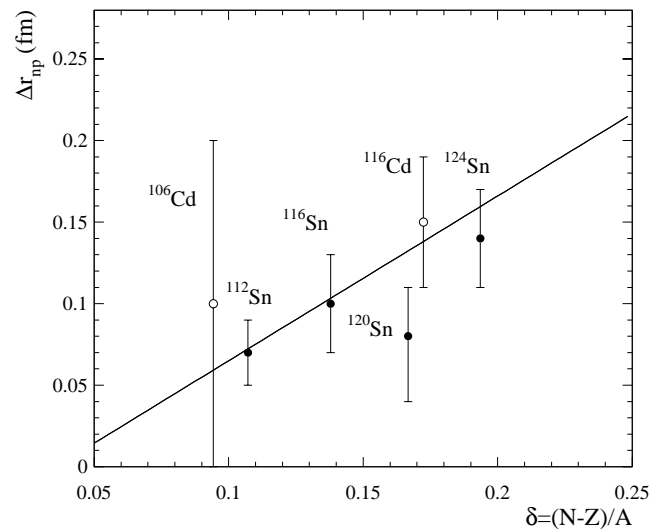

FIG. 8. Difference Δr_{np} between the rms radii of the neutron and proton distributions as deduced from the antiprotonic-atom x-ray data, as a function of $\delta = (N-Z)/A$. The full line is the same as in Fig. 5 of Ref. [9].

Different methods generally agree remarkably well in the determination of the first moment of the charge distribution, i.e., its rms radius. However, the situation is quite different in the nuclear periphery (around $\simeq 3\%$ of the central density) where the antiproton annihilation takes place. There 10–20 % differences between the charge density from various experiments are not an exception. A new value of the Δr_{np} for ^{124}Sn resulting from the present x-ray analysis is significantly smaller than the previously reported ones obtained with methods not depending on the charge distribution input [26,27,29,21]. This value is also smaller than would be expected from our radiochemical experiment (cf. Fig. 7). The experimental determination (or analysis) of higher moments of the charge distribution in this nucleus could perhaps clarify the observed discrepancies.

V. SUMMARY AND CONCLUSIONS

Antiprotonic x rays were measured in two even-*A* Cd and four even-*A* Sn nuclei. The strong-interaction level widths and shifts were determined. The contribution of the peripheral neutron densities to these observables was intestigated.

Our interpretation of the collected data was done using a simple two-parameter Fermi (2pF) model to describe the peripheral proton and neutron distributions. We verified that these simple distributions approximate rather well (within 20%) the distributions obtained from the HFB model in the region where the antiproton annihilation probability is significant. The parameters of the proton distributions were obtained from the literature, where 2pF charge distributions were determined from muonic-atoms or electron-scattering experiments.

For neutron-rich nuclei, the peripheral neutron distributions deduced from the antiprotonic x-ray data are in fair agreement with the earlier radiochemical experiments. This is, however, not the case for the lightest members of the investigated Cd and Sn isotope chains. In these nuclei the radiochemical data indicate enhanced peripheral proton density in comparison with the neutron density. This contradicts the x-ray data as well as the HFB model calculations. It may be explained by the formation of quasibound $\bar{p}p$ states in nuclei with weakly bound protons.

[1] C.J. Batty, Nucl. Phys. **A372**, 433 (1981).

[2] T. Köhler, P. Blüm, G. Büche, A.D. Hancock, H. Koch, A. Kreissl, H. Poth, U. Raich, D. Rohmann, G. Backenstoss, C. Findeisen, J. Repond, L. Tauscher, A. Nilsson, S. Carius, M. Suffert, S. Charalambus, M. Chardalas, S. Dedoussis, H. Daniel, T. von Egidy, F.J. Hartmann, W. Kanert, G. Schmidt, J.J. Reidy, M. Nicholas, and A. Wolf, Phys. Lett. B **176**, 327 (1986).

[3] C.J. Batty, E. Friedman, and A. Gal, Nucl. Phys. **A592**, 487 (1995).

[4] C.J. Batty, E. Friedman, H.J. Gils, and H. Rebel, Adv. Nucl. Phys. **19**, 1 (1989).

[5] S. Wycech, Nucl. Phys. **A692**, 29c (2001).

[6] J. Jastrzębski, T. Czosnyka, T. von Egidy, K. Gulda, F. Hartmann, J. Iwanicki, B. Ketzer, M. Kisieliński, B. Kłos, J. Kulpa, W. Kurcewicz, P. Lubiński, P. Napiorkowski, L. Pieńkowski, D. Santos, R. Schmidt, J. Skalski, R. Smolańczuk, A. Stolarz, A. Trzcińska, E. Widnamm, and S. Wycech, Nucl. Phys. **B56**, 108 (1997).

[7] F.J. Hartmann, R. Schmidt, T. von Egidy, J. Jastrzębski, P. Lubinski, L. Pieńkowski, A. Trzcińska, R. Smolańczuk, S. Wycech, and B. Kłos, Acta Phys. Hung. New Ser.: Heavy Ion Phys. **13**, 51 (2001).

[8] A. Trzcińska, J. Jastrzębski, T. Czosnyka, T. von Egidy, K. Gulda, F.J. Hartmann, J. Iwanicki, B. Ketzer, M. Kisieliński, B. Kłos, W. Kurcewicz, P. Lubiński, P. Napiorkowski, L. Pieńkowski, R. Schmidt, and E. Widmann, Nucl. Phys. **A692**, 176c (2001).

[9] A. Trzcińska, J. Jastrzębski, P. Lubiński, F.J. Hartmann, R. Schmidt, T. von Egidy, and B. Kłos, Phys. Rev. Lett. **87**, 082501 (2001).

[10] R. Schmidt, F.J. Hartmann, T. von Egidy, T. Czosnyka, J. Iwanicki, J. Jastrzębski, M. Kisieliński, P. Lubiński, P. Napiorkowski, L. Pieńkowski, A. Trzcińska, R. Smolańczuk, S. Wycech, B. Kłos, K. Gulda, W. Kurcewicz, and E. Widmann, Phys. Rev. C **58**, 3195 (1998).

[11] F.J. Hartmann, R. Schmidt, B. Ketzer, T. von Egidy, S. Wycech, R. Smolańczuk, T. Czosnyka, J. Jastrzębski, M. Kisieliński, P. Lubiński, P. Napiorkowski, L. Pieńkowski, A. Trzcińska, B. Kłos, K. Gulda, W. Kurcewicz, and E. Widmann, Phys. Rev. C **65**, 014306 (2002).

[12] J. Jastrzębski, H. Daniel, T. von Egidy, A. Grabowska, Y.S. Kim, W. Kurcewicz, P. Lubiński, G. Riepe, W. Schmid, A. Stolarz, and S. Wycech, Nucl. Phys. **A558**, 405c (1993).

[13] P. Lubiński, J. Jastrzębski, A. Grochulska, A. Stolarz, A. Trzcińska, W. Kurcewicz, F.J. Hartmann, W. Schmid, T. von Egidy, J. Skalski, R. Smolańczuk, S. Wycech, D. Hilscher, D. Polster, and H. Rossner, Phys. Rev. Lett. **73**, 3199 (1994).

[14] P. Lubiński, J. Jastrzębski, A. Trzcińska, W. Kurcewicz, F.J. Hartmann, W. Schmid, T. von Egidy, R. Smolańczuk, and S. Wycech, Phys. Rev. C **57**, 2962 (1998).

[15] R. Schmidt, F.J. Hartmann, B. Ketzer, T. von Egidy, T. Czosnyka, J. Jastrzębski, M. Kisieliński, P. Lubiński, P. Napiorkowski, L. Pieńkowski, A. Trzcińska, B. Kłos, R. Smolańczuk, S. Wycech, W. Pöschl, K. Gulda, W. Kurcewicz, and E. Widmann, Phys. Rev. C **60**, 054309 (1999).

[16] H. Koch, G. Poelz, H. Schmitt, L. Tauscher, G. Backenstoss, S. Charalambus, and H. Daniel, Phys. Lett. **28B**, 279 (1968).

[17] E. Borie, Phys. Rev. A **28**, 555 (1983).

[18] M. Leon and R. Seki, Phys. Rev. Lett. **32**, 132 (1974).

[19] M. Leon, Nucl. Phys. **A60**, 461 (1976).

[20] S. Raman, C.H. Malarkey, W.T. Milner, C.W. Nestor, Jr., and P.H. Stelson, At. Data Nucl. Data Tables **36**, 1 (1987).

[21] A. Trzcińska, J. Jastrzębski, P. Lubiński, F.J. Hartmann, R. Schmidt, T. von Egidy, and B. Kłos, Acta Phys. Pol. B **32**, 917 (2001).

[22] B. Kłos *et al.* (unpublished).

[23] J. Dobaczewski, H. Flocard, and J. Treiner, Nucl. Phys. **A422**, 103 (1984).

[24] H. de Vries, C.W. de Jager, and C. de Vries, At. Data Nucl. Data Tables **36**, 495 (1987).

[25] G. Fricke, C. Bernhardt, K. Heilig, L.A. Schaller, L. Schellenberg, E.B. Shera, and C.W. de Jager, At. Data Nucl. Data Tables **60**, 177 (1995).

[26] A. Krasznahorkay, A. Balanda, J.A. Bordewijk, S. Brandenburg, M.N. Harakeh, N. Kalantar-Nayestanaki, N.M. Nyako, J. Timár, and A. van der Woude, Nucl. Phys. **A567**, 521 (1994).

[27] A. Krasznahorkay, M. Fujiwara, P. van Aarle, H. Akimune, I. Daito, H. Fujimura, Y. Fujita, M. Harakeh, T. Inomata, J. Janecke, S. Nakayama, A. Tamii, M. Tanaka, H. Toyokawa, W. Uijen, and M. Yosoi, Phys. Rev. Lett. **82**, 3216 (1999).

[28] B. Nerlo-Pomorska, K. Pomorski, and J. Berger, Acta Phys. Pol. B **32**, 925 (2001).

[29] L. Ray, Phys. Rev. C **19**, 1855 (1979).